Isogeometric shape optimisation of volumetric blades for aircraft engines

Marie Guerder, A. Duval, T. Elguedj, Paul Feliot, Josselyn Touzeau

Structural and Multidisciplinary Optimization manuscript No.
(will be inserted by the editor)

Isogeometric shape optimisation of volumetric blades for aircraft engines

Marie Guerder · Arnaud Duval · Thomas Elguedj · Paul Feliot · Josselyn Touzeau

Received: date / Accepted: date

Abstract This papers presents a shape optimisation procedure within the framework of isogeometric analysis (IGA), applied to aircraft engine blades. A motivation for this work was the integration of geometric description, structural analysis and shape optimisation in a single industrial framework. As a matter of fact, the result of shape optimisation using IGA *is* a Computer Aided Design (CAD) model, proving itself quite advantageous in an industrial context. Our work takes as an input a stacked cross section definition of the blade geometry. Using B-Spline parametrisations, we reconstruct B-Spline analysis-suitable volumetric blade models. Several requirements – among which geometric accuracy and parametrisation regularity – are taken into account in this stage. The generated blade models are used to carry out structural shape optimisation. Static and dynamic cases are addressed, featuring relevant industrial loading cases such as centrifugal force and surface pressure yielded by aerodynamic simulations. Two different shape parametrisations are brought out for the shape optimisation, in order to modify the blade stacking axis or thickness. Compliance and natural frequencies are chosen as optimisation criteria. A natural frequencies case uses a B-Spline function in order to define the optimisation objective function.

Keywords Isogeometric analysis · Shape optimisation · Compressor blades · Trivariate B-Splines

✉ Marie Guerder
marie.guerder@insa-lyon.fr
[1] Univ Lyon, INSA-Lyon, CNRS UMR5259, LaMCoS, F-69621, France
[2] Safran Aircraft Engines, Site de Villaroche, 77550 Moissy-Cramayel, France

1 Introduction

Structural shape optimisation is widely used in mechanical engineering. Improving a geometry such that it complies with several constraints requires to integrate geometrical modelling, structural analysis and optimisation. This combination can reveal itself quite complex in terms of implementation, especially when considering that each of these three steps is usually carried out by means of different numerical tools and/or software.

The most commonly used framework for structural shape optimisation relies on multiple numerical models: a CAD model (or design model) to define the geometry and an analysis model to perform structural analysis, by means of finite element methods (FEM). Considering this configuration, two strategies arise: the first consists in using the CAD definition for the shape parametrisation (Imam, 1982; Braibant and Fleury, 1984), while the other uses the spatial location of nodes of a finite element mesh as design variables (Firl et al., 2013; Bletzinger, 2014). The CAD-based approach requires the re-meshing of the geometry for every new set of design variables. The FE-based strategy, apart from presenting a high number of design variables, can lead to distorted geometry. Mesh regularisation techniques can be employed to reduce this tendency, adding computational cost. Even though both techniques have drawbacks, they still are widely used in industrial frameworks. Seeking alternative methods to integrate the geometrical definition and the structural analysis is of high interest, especially in the context of structural shape optimisation.

Isogeometric analysis (IGA – see Cottrell et al. (2009) and Hughes et al. (2005)) offers a potential way out of the aforementioned limits. Its multilevel approach bringing together design and analysis, IGA reveals itself particularly suited for structural shape optimisation. This favourable feature has already been taken advantage of in various fields.

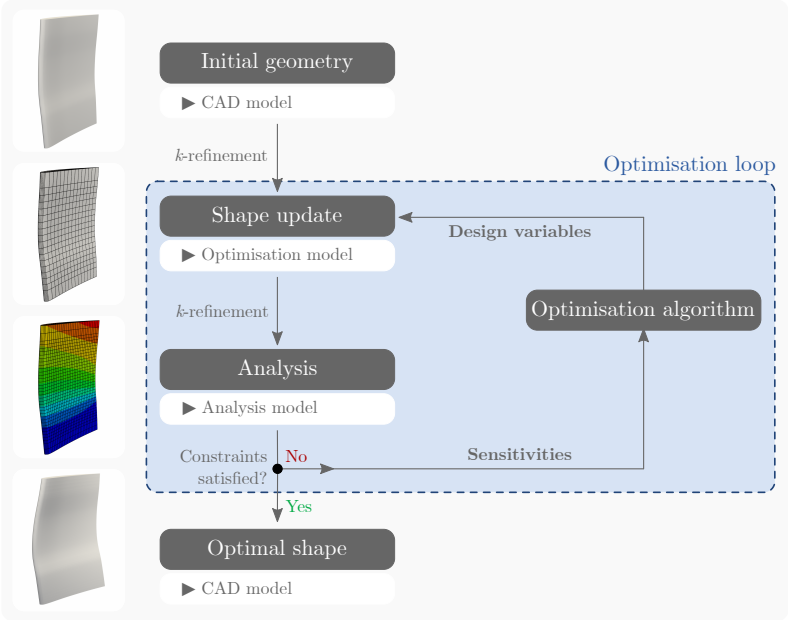

Fig. 1: Overview of the main steps of the isogeometric shape optimisation. A unique analysis-suitable geometric representation is used in such framework.

Fußeder et al. (2015), Wall et al. (2008) and Liu et al. (2019) introduced frameworks for IGA-based structural shape optimization for two-dimensional problems, using gradient algorithms for the optimisation. IGA is especially appropriate for gradient-based parametric shape optimisation, since the continuity of the geometry allows to compute the sensitivities analytically. Sensitivity analysis and computation of the derivative of the shape have been studied by Nagy et al. (2010) and Qian (2010) in two dimensions and by Blanchard et al. (2012); Hirschler et al. (2018) and Kiendl et al. (2014) in three dimensions. Works from Herrema et al. (2017) and Hsu et al. (2015) tackled the issue of integrating design, analysis and optimisation in a single framework. Regarding structural shape optimisation itself, classical criteria include compliance (Liu et al., 2019; Nagy et al., 2011) and natural frequencies (Ding et al., 2016; Ha, 2015; Kang and Youn, 2016).

Over the years, a general procedure for IGA-based shape optimisation has been drawn out. Figure 1 sums the main steps up. A single numerical representation is used to define the geometry and carry out structural analyses: the difference between the design and analysis models is a question of refinement level. The spatial location of the control points of the design model is usually used as design variables, while the analysis model presents an adequate refinement level to guarantee the quality of the solution.

Considering the aircraft engines field, integrating design and analysis in a single framework is one of the aspects leading to the exploration of IGA. Another crucial feature is the transition from the shape optimisation resulting model back to the CAD environment. This conversion is essential for manufacturing purposes. What is more, describing the initial geometry of blades thanks to parametric curves such as B-Splines or Non-Uniform Rational B-Splines (NURBS) has already been explored, not only for aicraft engines blades (Großmann and Jüttler, 2010; Mykhaskiv et al., 2018), but also wind turbines blades (Stein et al., 2012; Herrema et al., 2017), or marine propellers (Pérez-Arribas and Pérez-Fernández, 2018; Arapakopoulos et al., 2019).

Given the aforementioned elements, using IGA in the context of aircraft engines blades design and optimisation seems an interesting choice. A tackled issue in this work is the generation of a volumetric B-Spline blade model that is parametrically suitable for both analysis and shape optimisation purposes, given a series of stacked blade cross-sections as an input. Another matter we bring to light is to carry out structural analysis onto trivariate B-Spline blade models featuring actual industrial loading cases. We emphasise this work addresses the question of aircraft engines blades mechanical design, for which the criteria that are used mainly consist in dynamic ones. Hence, the vibration behaviour of two blades is studied, along with the compliance of one of them. Then, we perform shape optimisation of two blade models, using a total of three different objective functions. The first is the expression of compliance, as classically studied in structural shape optimisation. The second and third are set to act on natural frequencies. In particular, we defined an objective function expressed by a sum of B-Spline function values.

Section 2 introduces notions about isogeometric analysis and shape optimisation. Section 3 consists in our framework for generating a trivariate B-Spline blade model, as well as some elements concerning blade geometrical design. In section 4 we present the trivariate blade models we use in the rest of this paper along with some preliminary analyses of

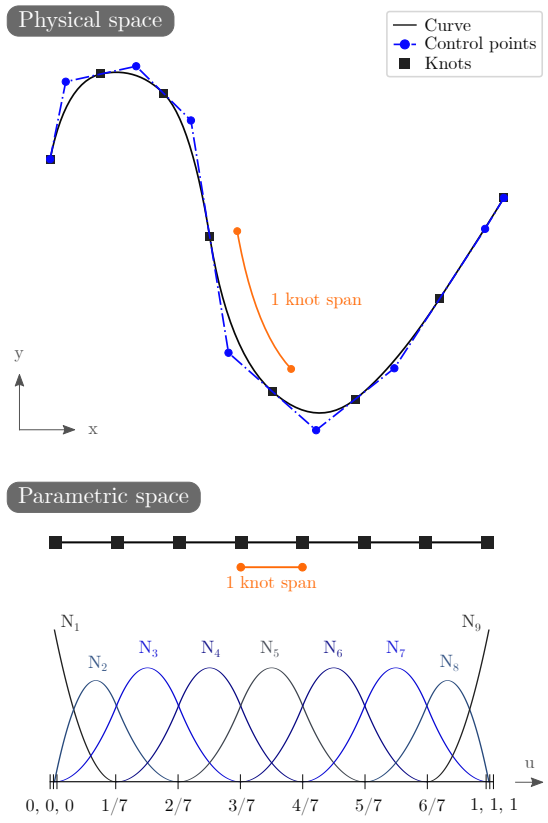

Fig. 2: Physical and parametric spaces for a quadratic B-Spline curve in $\mathbb{R}^2$. The associated knot vector is defined as $U = \{0, 0, 0, 1/7, 2/7, 3/7, 4/7, 5/7, 6/7, 1, 1, 1\}$.

the blades. Section 5 features the shape optimisation set-up we used and various numerical examples[1]. Section 6 ends this article with some concluding remarks and possible improvements.

2 Background

2.1 B-Splines and Isogeometric Analysis

A few aspects about B-Spline objects and their properties are given hereafter. The interested reader can refer to the *NURBS book* by Piegl and Tiller (1995) for example for more details.

A B-Spline curve $\mathbf{C}$ of degree p in $\mathbb{R}^{2,3}$ is defined as

$$\mathbf{C}(u) = \sum_{i=0}^{n} N_{i,p}(u)\,\mathbf{P}_i, \tag{1}$$

where the $\{N_{i,p}\}_{1\leq i\leq n}$ are n B-Spline basis functions, $n \in \mathbb{N}$, the $\{\mathbf{P}_i\}_{1\leq i\leq n}$ are n control points in $\mathbb{R}^{2,3}$ and u is a parameter on an interval $U \subset \mathbb{R}$. B-Spline basis functions are computed recursively using the Cox-de-Boor formula (Cox, 1972; De Boor, 1972). A B-Spline basis function is defined in the parametric space by its *knot vector* U, which is an ordered list of parameters. The number of knots is linked to the degree p and the number of control points n of the curve. If the knot values are uniformly spaced, the knot vector is said *uniform*; otherwise it is *non-uniform*.

For multi-dimensional approximations, the basis functions are defined as a tensor product of one-dimensional basis functions. For example, given a control net $\{\mathbf{P}_{i,j,k}\}_{i,j,k}$ of points in $\mathbb{R}^3$, degrees p, q, and r and intervals U, V and W with associated knot vectors, a B-Spline solid is defined on $U \times V \times W$ as:

$$\mathbf{S}(u,v,w) = \sum_{i=1}^{n}\sum_{j=1}^{m}\sum_{k=1}^{l} N_{i,p}(u)\,M_{j,q}(v)\,L_{k,r}(w)\,\mathbf{P}_{i,j,k}. \tag{2}$$

A significant aspect when considering the formulation of a B-Spline geometry is the differentiation between the so-called *parametric* and *physical* spaces. The first is the place where knots are defined, whereas the latter is where the control points are spanned, and hence where the curve, surface or solid lies. Knots are delimiting the so-called *knot spans* in parametric space, which can be taken for elements in a finite elements sense. Still, one must be aware that a uniform knot vector will not necessarily span regularly spaced elements in physical space, *e.g.* see figure 2.

Introduced by Hughes et al. (2005), IGA is a numerical method that aims at improving the link between geometrical design and analysis. It relies on the use of B-Splines or Non-Uniform Rational B-Splines (NURBS) functions in order to represent both the geometry and to carry out analysis. Hence, as in standard Finite Element Methods, the isoparametric concept is invoked. The core difference between the two approaches is that IGA yields an exact representation of the geometry to compute the unknown fields during analysis, while in classical Finite Elements Methods the mesh actually approximates the geometry. Another attractive feature of IGA lies in its computational precision, partly brought by the higher continuity of B-Spline functions, in comparison with Lagrange polynomials for instance. B-Spline functions present other interesting properties to be used in the IGA framework, such as efficient refinement procedures.

2.2 Parametric shape optimisation

Mathematically, optimisation consists in minimising an objective function f, subject to constraints $\{c_i\}$ and $\{e_i\}$ on its variables x – often called *design variables* in structural

[1] We emphasise that the presented quantitative results are dimensionless, for non-disclosure matters. The normalised values μ^* are computed as follows: $\mu^* = (\mu - \mu_{min})/(\mu_{max} - \mu_{min})$, where μ is the initial value, and μ_{max} and μ_{min} the maximum and minimum values of the considered dataset, respectively.

shape optimisation. The optimisation problem can then be expressed as follows: Formally, given a d-dimensional *design space* $\mathbb{X} \subset \mathbb{R}^d$ and an *objective function* $f : \mathbb{X} \to \mathbb{R}$ to be minimized, a parametric optimisation problem can be defined as follows.

$$\text{Find } x^\star = \underset{x \in C}{\operatorname{argmin}}\, f(x), \tag{3}$$

where $C = \{x \in \mathbb{X} \,|\, c_i(x) \leq 0, e_j(x) = 0, (i,j) \in \mathscr{I} \times \mathscr{J}\}$ is an admissible subdomain of $\mathbb{X}$ defined by real valued inequality constraints $(c_i)_{i \in \mathscr{I}}$ and equality constraints $(e_j)_{j \in \mathscr{J}}$ defined on $\mathbb{X}$, where $\mathscr{I}$ and $\mathscr{J}$ are sets of indices.

Several methods can be used in order to solve the optimisation problem (3). The interested reader is referred to Nocedal and Wright (2006) for a comprehensive review on continuous gradient-based optimisation. In the numerical experiments presented in this article, we used a Sequential Quadratic Programming (SQP) algorithm based on Kraft's implementation (Kraft, 1994) and available as the `SLSQP` method in the `optimize` module of the open-source `SciPy` library for non-linear optimisation (Virtanen et al., 2020). This gradient-based algorithm can handle optimisation domains defined using bound constraints as well as both non-linear inequality and equality constraints.

Expressing the gradients of the objective function and of the constraints with respect to the design variables of the optimisation problem is a key aspect when using a gradient-based algorithm, which can lead to tedious developments. When these are not available, because they cannot be formally expressed or because it would be too difficult to do so, one way of getting around the issue is to use a finite-differences scheme or an automated differentiation method (Bischof et al., 2008; Bücker et al., 2006). In our case however it is not necessary, as IGA proved itself well conditioned for computing analytically the values of interest for the investigated cases. In particular, the isogeometric approach lends itself well to sensitivity analysis thanks to the continuity of the geometry; see Cho and Ha (2009) for more details on this aspect. A detailed summary of all required steps for the computation of analytical sensitivities using IGA for various objective functions is given in Hirschler et al. (2020).

3 A trivariate B-Spline model for 3D blades

In this section, we give a few elements of context about the geometrical definition of blades in an industrial environment, with a focus on axial compressor blades. Then, we propose a generic framework to build single-patch volumetric B-Spline blade models that are compatible with IGA.

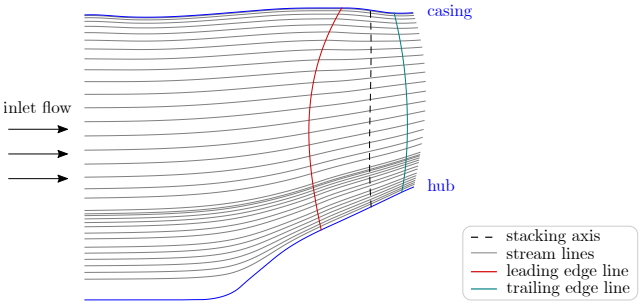

Fig. 3: Two-dimensional stream lines in a low-pressure axial compressor. The leading and trailing edges lines of the fan blade are represented as well.

3.1 Axial compressor blades geometrical design

When designing aircraft engines axial compressor blades, a common practice in industry lies in tackling aerodynamics and structural mechanics issues separately. Most of the time, these two aspects are actually addressed by different specialised teams. A blade geometry is usually defined by modelling solely its outer surface. It is defined by a series of cross-sections or *profiles*, that are stacked along the blade height. The number and geometries of the profiles as well as the way they are stacked are as many design choices that aerodynamic and mechanical teams have to agree upon.

The behaviour of the air flow passing through an axial compressor can be represented by *stream lines* (or *flow lines*, see figure 3), which are typically obtained using Euler-2D aerodynamic analyses. A revolution of these flow lines about the engine's rotation axis is usually performed to define three-dimensional stream surfaces. The profiles are then drawn in 2D and a conformal operation onto the stream surfaces is done to yield blade sections defined in 3D space. These are then lofted along a *stacking axis* to build the blade three-dimensional geometry. For more details on surface lofting see Piegl and Tiller (1995).

An example of stacked cross-sections is shown in the Step 1 of figure 5. These curves are the starting point for the generation of the trivariate B-Spline blade model.

3.2 Trivariate model generation

The first milestone of this work towards isogeometric shape optimisation of blades consists in generating an analysis-suitable volumetric B-Spline model of blades that is also suitable for optimisation. Namely, the geometrical description of the blade must present reasonable (*i.e.*, not too high) degree and number of control points, while being sufficiently fine to describe the input geometry finely. The repartition of the knots spanned in the physical space is also an important aspect: we seek to obtain a smooth knots distribution in all

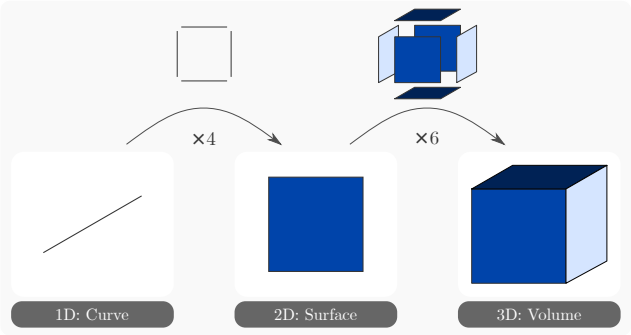

Fig. 4: Illustration of the essential geometric operations resulting in a volumetric cube.

three physical directions. The quality of the solution (when running structural analyses for instance) can later be insured *via* refinement operations, see Cottrell et al. (2007) for instance.

When it comes to generate a trivariate B-Spline model, several strategies arise in terms of number and spatial organisation of patches. In our case, the topology of a blade lends itself well to consider a single-patch model. To do so, we assume that the geometry of the blade is homomorphous to a cube, as illustrated in figure 4. In a nutshell, we seek to identify the basic geometric elements for obtaining a cube: four curves in order to form a closed surface, and then six surfaces in order to assemble a closed volume. The choice of this strategy entails a number of geometrical manipulations, some of which have already been tackled by Großmann and Jüttler (2010) for instance.

The methodology that we propose to generate a volumetric blade model is outlined in figure 5. Its main steps are listed hereafter.

1. Create the set of 3D B-Spline curves forming the stacked blade profiles.
2. For each of these curves, identify four *wedge points* and split each profile accordingly. This step yields four (stacked) curves groups: leading edge, pressure side, trailing edge and suction side.
3. Adjust the parametrisation of all created curves.
4. Create four surfaces from the four curves groups generated in step 2 (the so-called *contour* surfaces).
5. Adjust the parametrisation of the surfaces.
6. Create the two missing surfaces, *i.e.*, *top* and *bottom* surfaces, by interpolating linearly the curves forming the first and last profiles.
7. Compute the volume control points by linear combination of the control points of the six outer surfaces.

Throughout the rest of this section the reader may refer to figure 5 to picture the described operations more clearly.

Step 1 – Initial curves. Our starting point is a series of B-Spline curves describing the blade's geometry as stacked aerodynamic profiles. These curves thereby define the outer surface of the blade only.

Step 2 – Curve splitting. In order to assimilate each profile to a square, the location of the supposed four corners first has to be defined. To this end, we chose the same method as Großmann and Jüttler (2010) for identifying the *wedge points* (see figure 6). First, the points forming the tip of the profile are fitted to a sphere by means of an iterative method. Starting from the foremost point, *i.e.*, *edge point*, one point is added on each side at every step, and the resulting fit error is computed. The loop stops when the fit error exceeds a user-defined tolerance. Once the *wedge points* are identified for all profiles, the curves are split using multiple knot insertion. This step yields four curves groups, gathered by profile parts.

Step 3 – Curves re-parametrisation. One requirement for creating a surface from curves is the compatibility between them, especially in terms of parametric definition. In our case all curves belonging to the same group must be described on the same knot vector and be of the same degree. Another concern in this work is the repartition of the curves' knots in physical space, for ensuring the regularity of the final isogeometric mesh. To fulfil both these conditions, the chosen approach combines two algorithms. An overview of the process is pictured in figure 7.

The first step is to compute a parameters sequence such that, when used for evaluating a curve, it results in evenly spaced physical points. To this end, we used the **UniArcLength** algorithm from Hernández-Mederos and Estrada-Sarlabous (2003). It precisely complies with our needs by computing a sequence of parameters yielding regularly spaced points in physical space, see the *Sampling* step in figure 7. In this algorithm, values of the parameters are computed using arc length parametrisation.

Then, the regularly spaced physical points are used for curve approximation, using a classical curve fitting algorithm from Piegl and Tiller (1995). On the one hand, using approximation instead of interpolation enables to choose the number of control points of the resulting curve as well as its degree; on the other end, having regularly spaced points as input yields regularly spanned knots in physical space.

Step 4 – Contour surfaces creation. The creation of the so-called *contour* surfaces is straightforward. Given a set of compatible curves, the control points of the surface are defined as those of the curves. Considering the parametric aspects, one parametric direction naturally inherits its knot vector and degree from the curves. For the other direction (the stacking direction), a uniform knot vector is used. Hence, another re-parametrisation step is required.

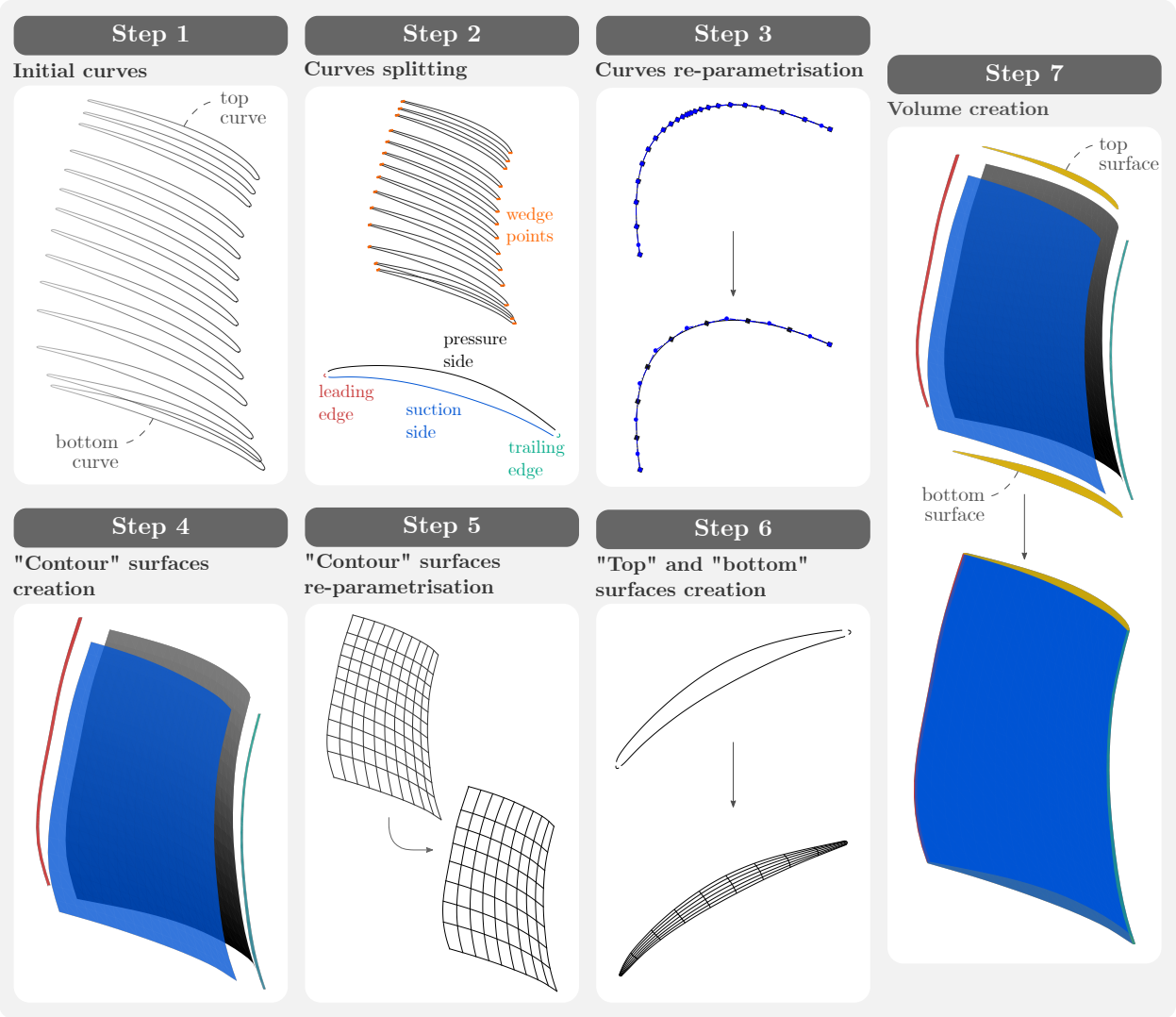

Fig. 5: Overview of the framework for volumetric reconstruction of the blade. Steps 1 to 3 consist in curves processing operations, while steps 4 to 6 apply to surfaces. Finally, step 7 is about the creation of the final volume.

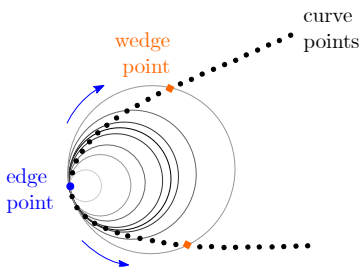

Fig. 6: Schematic view of the process of fitting the edge points to a sphere. The operation is illustrated in the 2D case for clarity.

Step 5 – Contour surfaces re-parametrisation. This step is analogous to step 3. The objective is to obtain knots regularly spanned in the stacking direction, *i.e.*, the blade's height. To that end we use a skinned surface (see Piegl and Tiller (1995)), which enables to obtain the desired degree, number of control points and knots repartition in the direction of interest.

Step 6 – Top and bottom surfaces. Two surfaces are missing in order to complete the set of six surfaces needed to create a volume as pictured in figure 4. These two surfaces are the *top* and *bottom* ones, respectively based on the first and last profile of the blade. They are created by using bilinear interpolation of the boundary curves, namely a Coons patch (Coons, 1967). The resulting surfaces are already well parametrised (in the sense of parametric description and knot spacing) since their boundary curves have already been processed in step 3.

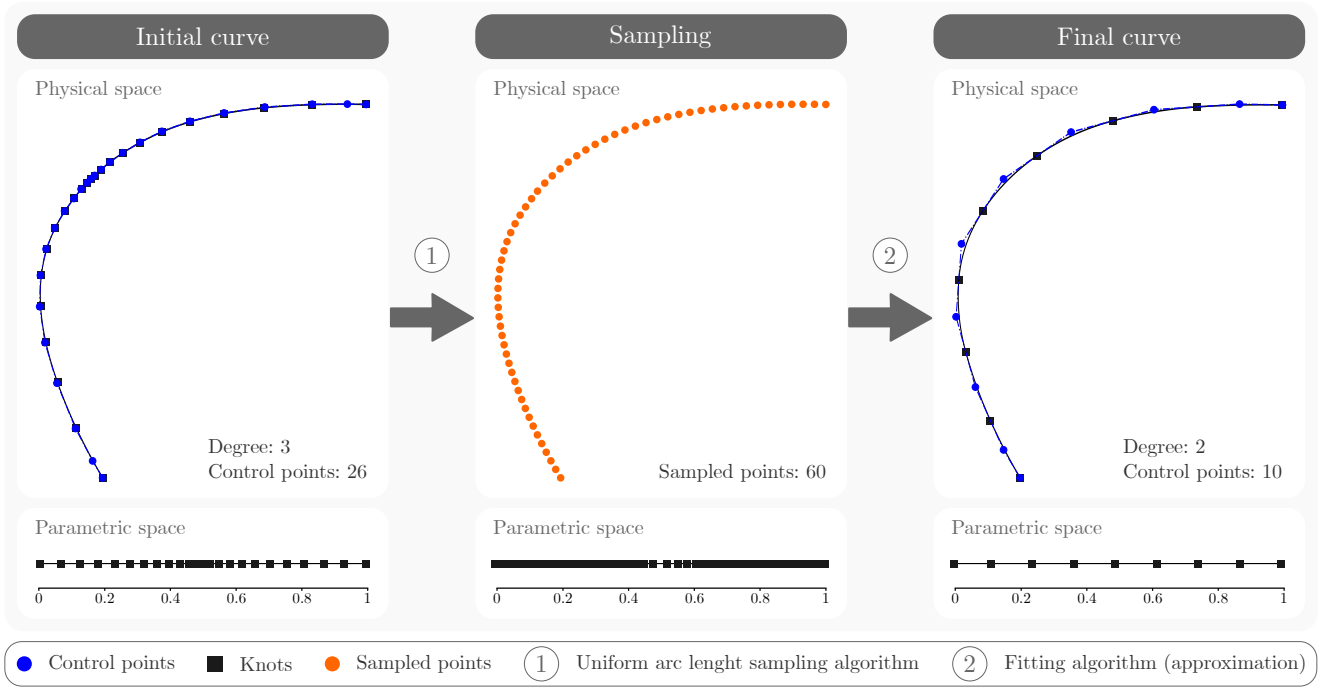

Fig. 7: Curves re-parametrisation steps. The process is illustrated for a leading edge curve; here the interest of obtaining a coarser parametrisation appears clearly.

Step 7 – Volume creation The last step consists in generating the inner control points of the trivariate B-Spline model. Their coordinates are computed by linear interpolation of the control points of the boundary surfaces, using the trivariate generalisation of a Coons patch. The detailed expression can be found in Xu et al. (2011), based on Farin and Hansford's work Farin and Hansford (1999). The position of interior control points can then be adjusted if necessary, see Xu et al. (2011) for instance.

4 Isogeometric analysis of compressor blades

4.1 Geometrical models

The methodology detailed in section 3 is now applied on geometries representative of a low-pressure compressor fan blade and of an high-pressure (HP) compressor rotor blade. The resulting models are illustrated in figure 8. They are used in sections 4.2 and 4.3 to perform a static and a dynamic analysis using IGA.

We chose these two blade geometries in order to highlight various aspects of this work. First, the two blades present different levels of geometrical complexity. The HP compressor blade is small in height and does not present a highly "folded" geometry. On the contrary, the fan blade is rather slender and highly twisted. Note in particular the difference of scale between the two geometries, which is highlighted in figure 8, and the uniformity of the resulting meshes, which is a product of the reparametrisation steps detailed in 3. The proposed methodology dealt well with both geometries, which highlights its overall robustness and genericity.

Furthermore, the function and the position of the two blades in the engine will allow us to explore different test cases, with different design criteria in each case, as detailed in section 5. Also, the potential for improvement using shape optimisation is not the same for both geometries. The HP compressor blade is an actual blade geometry, so its potential for improvement is not very high since its shape is already quite optimal. The fan blade on the other hand, is still at a development stage and offers more room for improvement using shape optimisation techniques.

4.2 Compliance analysis

Minimising compliance is a common objective in structural shape optimisation. The novelty of our work lies in the type of loadings applied to the geometry, namely a centrifugal force and an actual pressure field resulting from aerodynamic simulations, which is illustrated in figure 9. These two loadings are the most relevant for the mechanical sizing of engine blades. Only the HP compressor blade is considered here and the analysis set-up is as follows. The blade's bottom face ($z = 0$) is fixed. The engine rotation speed is set to 15768 rpm, which corresponds to a typical cruise flight

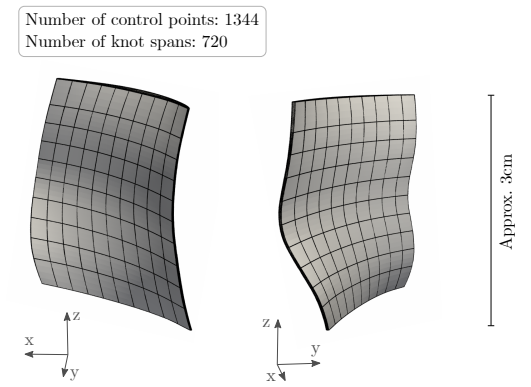

(a) HP compressor blade.

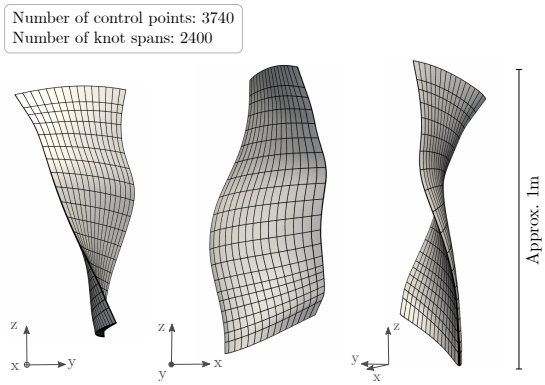

(b) Fan blade.

Fig. 8: Final volumes with parametric lines.

condition. The pressure field is the one illustrated in figure 9. The computation gives a compliance value equal to $12.62 m/N$.

4.3 Dynamic analysis and Campbell diagram

The dynamic analysis of compressor blades is crucial to their mechanical design. During their lifetime, both rotor and stator blades are subject to numerous vibration excitement sources due to the engine's rotation. All phases of a flight imply different velocities, creating various excitement frequencies; blades must fulfil their function during every flight phase. Their dynamic behaviour is thus extensively studied in practice and a series of criteria taking the form of frequency safety margins are used.

The first excitation sources to take into account are linked to the frequency harmonics of the engine rotation speed : 1N, 2N, 3N... Where N is the engine's operating speed. These excitation sources are particularly important for blades with low natural frequencies. It is the case for the fan blade for example, which is quite slender and has its first natural frequency around $40 Hz$. The second excitation source is related to the harmonic frequencies of the engine corresponding to the number of blades on the same stage and/or on neighbouring stages of the studied blade. Additional rules exist, whether the blade is mobile or fixed, but these are not considered in this work. Blades with high natural frequencies are more subject to this type of excitement. The HP compressor blade belongs to this category, with a first vibration mode around $2100 Hz$, which is noticeably higher than the fan blade for instance.

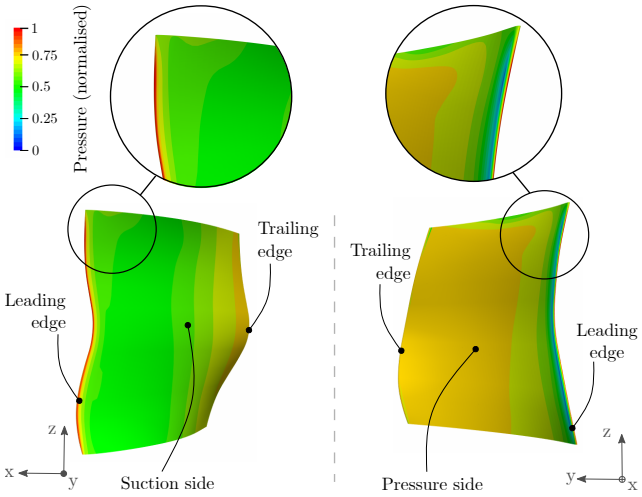

Fig. 9: Illustration of the pressure field applied on the HP compressor blade outer surface.

Whichever is the excitement source and the value of the associated frequency, a safety margin of 15% is commonly used. Therefore, given a rotation speed and an excitation source, a safety range can be defined around the associated frequency. The goal is then to prevent the blades from having any natural frequencies lying in that range.

A usual way of visualising the frequency interactions of the blade/engine system is to draw a Campbell diagram (Campbell, 1924), also called an *interference diagram*, see figure 10. Natural frequencies of the blade are drawn along with the rotation speed of the engine for a particular operation regime, and the harmonic(s) of interest.

As in the static case, the bottommost face of the blade is kept fixed in our analysis. For the HP compressor blade we chose to plot an arbitrary harmonic, namely 30N. Looking at figure 10a, one can notice the third natural frequency of the blade is lying in the safety margin associated with this particular harmonic. For the fan blade (illustrated in 10b), only the first harmonic, *i.e.*, 1N, is drawn. It is clear that the fifth natural frequency does not comply with the 15% margin requirement, while the fourth natural frequency is at the border of the range. A general observation is that the natural frequencies values for both blades are unaffected by the value of the rotation speed. In practice, this is not the case since cyclic symmetry has a great influence on the vibration

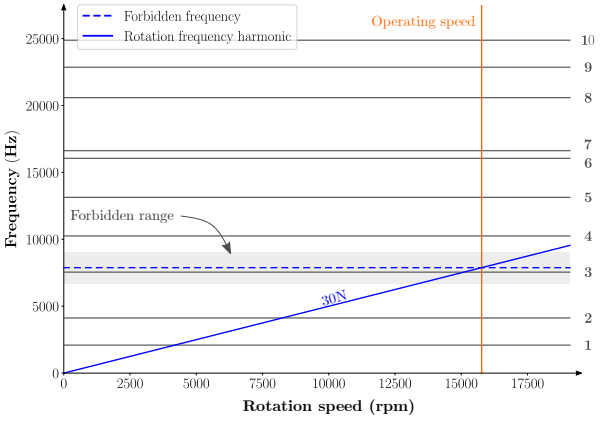

(a) HP compressor blade.

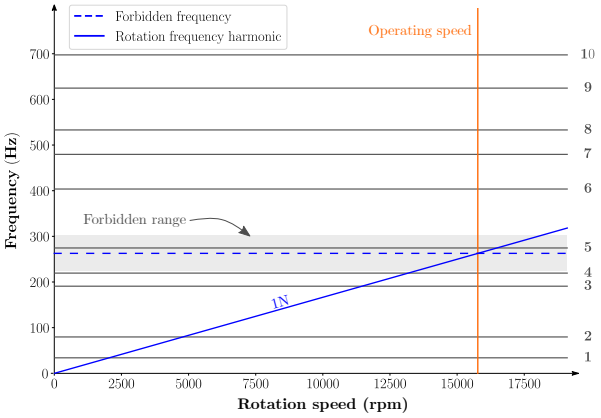

(b) Fan blade.

Fig. 10: Initial Campbell diagrams of the HP compressor (a) and fan (b) blades. The dashed line represents the frequency value we seek to avoid. This value corresponds to a given harmonic of the rotation speed we consider (vertical orange line on the figures). The shaded area corresponds to a 15% margin around this value. The indices on the right-hand part of the diagrams correspond to the vibration modes indices.

behaviour of the system. However, this phenomenon is not taken into account in the analysis setup we consider.

5 Shape optimisation of compressor blades

Three different sizing cases are considered in this section. The fist one is a classical case of compliance minimisation under volume constraint. The second case is a target attainment problem where the objective is to achieve particular values for certain natural frequencies. The third case takes the form of a forbidden frequency problem where the objective is to move certain natural frequencies out of forbidden ranges of values. A B-spline based objective function formulation is proposed in that case.

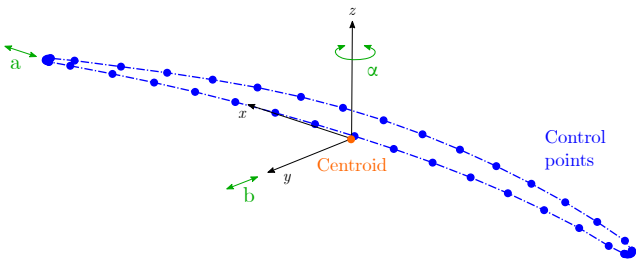

Fig. 11: Illustration of the authorised motions for one section for the stacking axis shape parametrisation. Only the exterior control points of the section are represented for clarity.

5.1 Parametric shape modifications

In this work, two parametric shape modifications are set up. The first modifies the stacking law of the blade sections. It is used in the compliance minimisation case in section 5.2. The second modifies the thickness of the blade sections[2] and is used for the target frequency and forbidden frequency problems of sections 5.3 and 5.4.

5.1.1 Stacking law modification

This first parametric shape modification is set up to control the position and orientation of the sections along the height of the blade. It is used on the HP compressor blade in the compliance minimisation case in section 5.2.

For each section of the blade, a geometric centroid is computed in order to define the origin of a local coordinate system. Three types of motion are defined : two translations along the x and y axes, and one rotation along the z-axis. These are parametrised using variables a, b and θ respectively, as illustrated in figure 11.

Let us denote by $\mathbf{R}$ the rotation matrix of angle θ along the z axis,

$$\mathbf{R} = \begin{pmatrix} \cos\theta & \sin\theta & 0 \\ -\sin\theta & \cos\theta & 0 \\ 0 & 0 & 1 \end{pmatrix}, \tag{4}$$

and by $\mathbf{T} = (a, b, 0)^T$ the translation vector. Given an initial control point $\mathbf{P} = (x, y, z)^T$, the application of the shape parametrisation yields a modified control point $\tilde{\mathbf{P}}$ which coordinates are computed as

$$\tilde{\mathbf{P}} = \mathbf{R} \cdot \mathbf{P} + \mathbf{T}. \tag{5}$$

[2] Both modifications are based on sections along the height of the blade. Here we consider sections that correspond to rows of control points after re-parametrisation. Therefore, there is no link between the considered sections and the initial ones, that are based on stream surfaces.

The derivatives of equation 5 with respect to the design variables a, b and θ can therefore be computed using the following formulas.

$$\begin{cases} \dfrac{\partial \tilde{\mathbf{P}}}{\partial a} = (1,0,0)^T \\ \dfrac{\partial \tilde{\mathbf{P}}}{\partial b} = (0,1,0)^T \\ \dfrac{\partial \tilde{\mathbf{P}}}{\partial \theta} = \dfrac{\partial \mathbf{R}}{\partial \theta}\mathbf{P} \end{cases} \tag{6}$$

with

$$\frac{\partial \mathbf{R}}{\partial \theta} = \begin{pmatrix} -\sin\theta & \cos\theta & 0 \\ -\cos\theta & -\sin\theta & 0 \\ 0 & 0 & 0 \end{pmatrix}. \tag{7}$$

Looking at equation (6), one can note that the derivatives of the shape parametrisation with respect to the translation variables are constant but that its derivatives with respect to θ is not. Therefore it has to be recomputed for each sensitivity evaluation during the optimisation process.

Since no aerodynamic constraints are taken into account in this work, bound constraints are defined in order to avoid consequential shape modifications from an aerodynamics point of view. Hence, for each blade section, bounds are set on all three design variables: the rotation angle θ will be set between ± 2 degrees, while the translations a and b will be set between ± 1 mm.

5.1.2 Thickness modification

The second parametric shape modification is set up to control the thickness of the sections along the height of the blade. It is used for the target frequency and forbidden frequency problems of sections 5.3 and 5.4.

The principle of the parametrisation is illustrated in figure 12. The goal is to enable thickness variations by using directly the control points' location. In order to vary the thickness, the control points forming the section's suction and pressure sides are paired. Each pair forms a line from which a unit direction vector can be defined. Then, a variable α attributed to each pair is used to control the magnitude of the translation of the pair of control points in opposite directions along this unit vector.

Formally, the expression of this shape parametrisation can be expressed as

$$\begin{cases} \tilde{\mathbf{P}}_0 = \mathbf{P}_0 + \alpha \mathbf{e} \\ \tilde{\mathbf{P}}_1 = \mathbf{P}_1 - \alpha \mathbf{e} \end{cases} \tag{8}$$

where $(\mathbf{P}_0, \mathbf{P}_1)$ is a pair of control points, $(\tilde{\mathbf{P}}_0, \tilde{\mathbf{P}}_1)$ is the same pair after transformation, $\mathbf{e}$ is the unit direction vector

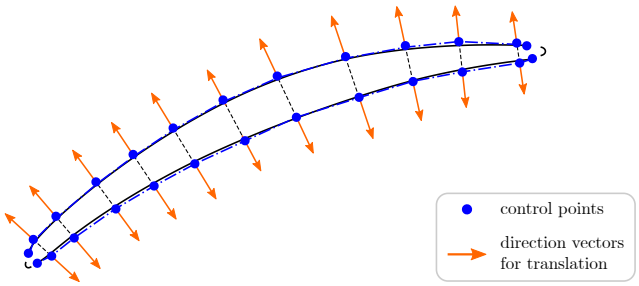

Fig. 12: Illustration of the motion of paired control points on one section for the thickness shape parametrisation.

associated with the pair, and α is the magnitude of the translation, which is the same for both points in order to preserve the blade's skeleton.

The derivatives of (8) with respect to the design variable α can be computed using the following formula, with $k \in \{1,2\}$,

$$\frac{\mathrm{d}\tilde{\mathbf{P}}_k}{\mathrm{d}\alpha} = \pm \mathbf{e}. \tag{9}$$

Since the shape parametrisation modifies the thickness of the blade, the bound contraints applied on the α variables for each section and each pair of control points are an important aspect of the optimisation problem setup. Indeed, it is necessary to avoid unfeasible geometries as much as possible, especially regarding crafting matters. Hence, the bounds on the design variables are defined such that the resulting thickness of the blade in any modified location can neither be greater than the initial highest value nor smaller than the initial lowest value.

5.2 Compliance minimisation

We first consider the minimisation of the compliance under a volume constraint for the HP compressor blade. Its volume V is allowed to vary by at most 10% of its initial value V_0, which is formalised as a single inequality constraint

$$c(x) = (V(x) - 0.9V_0)(V(x) - 1.1V_0), \quad x \in \mathbb{X}. \tag{10}$$

The parametric stacking law modification described in section 5.1.1 is considered. The two bottommost sections are fixed and the remaining ten sections are allowed to vary, resulting in a total of $3 \times 10 = 30$ design variables for this case.

The simulation model is the same as in section 4.2. The displacement fields and stacking axis of the blade before and after the optimisation are illustrated in figures 13 and 14 respectively. The values of θ for each section are also shown on the figure for comparison

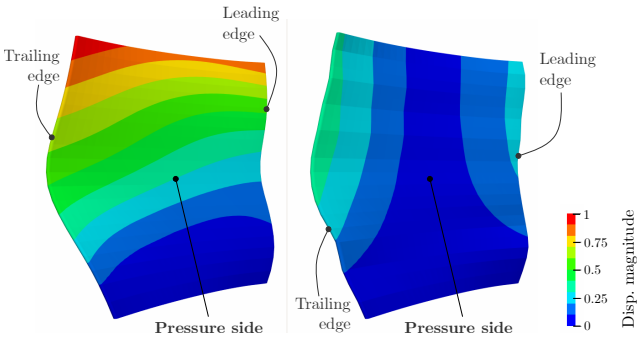

Fig. 13: Displacement fields for the initial (left) and optimised (right) geometries after compliance optimisation on the HP compressor blade.

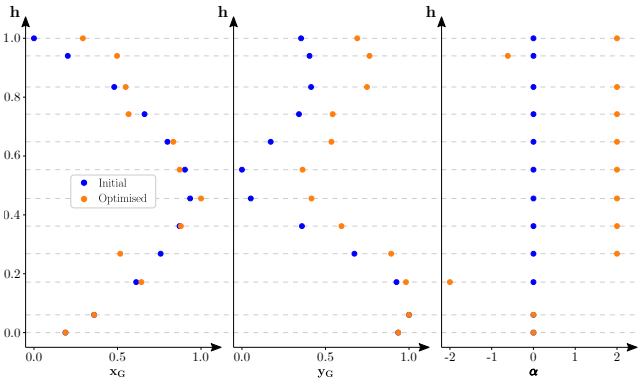

Fig. 14: Comparison of the initial and optimised stacking laws. The dots represent the centroids of the blade sections. The x-coordinates are plotted on the left-hand graph, and the y-coordinates on the middle one. Both are plotted along the (normalised) height of the blade. On the rightmost part of the figure are displayed the θ values.

One can observe that the displacements have been significantly reduced by the optimisation. As a consequence, the compliance value has dropped by 40%. Even though the final shape is not realistic from an aerodynamic point of view, we believe that this example effectively demonstrates the feasibility of the approach.

5.3 Target frequencies

We now turn to the target frequencies problem. The preliminary analyses of section 4.3 revealed two problematic natural modes for each blade, that will be the starting points of our investigations. Table 1 sums up the initial and targeted frequency values for the HP compressor blade and for the fan blade.

The following objective function is considered for this problem,

$$f(x) = \sum_{i=1}^{2} \left(\frac{\omega_i(x) - \omega_{i,\text{target}}}{\omega_{i,\text{target}}} \right)^2, \tag{11}$$

HP compressor blade			
Mode no.	Initial	Target	Final
3	7550 Hz	6365 Hz	6366 Hz
4	10250 Hz	9530 Hz	9532 Hz
Fan blade			
Mode no.	Initial	Target	Final
4	219 Hz	220 Hz	220 Hz
5	275 Hz	305 Hz	305 Hz

Table 1: Initial, targeted and final frequencies for the modes of interest for the HP compressor blade and for the fan blade.

where the $(\omega_{i,\text{target}})_{i\in\{1,2\}}$ are target eigen pulsation values and the $(\omega_i(x))_{i\in\{1,2\}}$ are the eigen pulsation values of a blade modified according to x. Practically, this objective function favours precise target frequency values for the two selected modes. Besides, the same volume constraint (10) as in the compliance minimisation case is enforced. We emphasise that the analysis steps during the optimisation process does not take the rotational speed into account when computing the eigen frequency values. The parametric thickness modification described in section 5.1.2 is considered. The HP compressor blade is made of 12 sections, with 12 direction vectors each, which makes a total of 144 design variables. The fan blade on the other hand, is made of 22 sections with 15 direction vectors each, which makes a total of 330 design variables. The simulation model is the same as in section 4.3. The final values of the natural frequencies for the modes of interest are reported in table 1 and the thickness repartition of the initial and optimised geometries are illustrated in figures 15 and 16, for the HP compressor blade and for the fan blade respectively. As expected, the final frequencies are very close to the target values. The optimised HP compressor blade tends to be thinner than the initial one, except for the middle and top sections, which are thicker. As a result, the volume of the blade has dropped by 9%. As regards the fan blade, it is globally slightly thinner, with certain zones of greater thickness, especially on the top sections near the leading edge. Its final volume is 3% greater than the initial one.

5.4 Forbidden frequencies

Satisfying results were obtain with the target frequencies formulation of section 5.3. However, using target frequencies is not practical when a high number of natural frequencies have to be constrained, or when it is desirable to avoid multiple frequency ranges simultaneously. To address these limitations, we propose a second formulation with a different definition for the objective function.

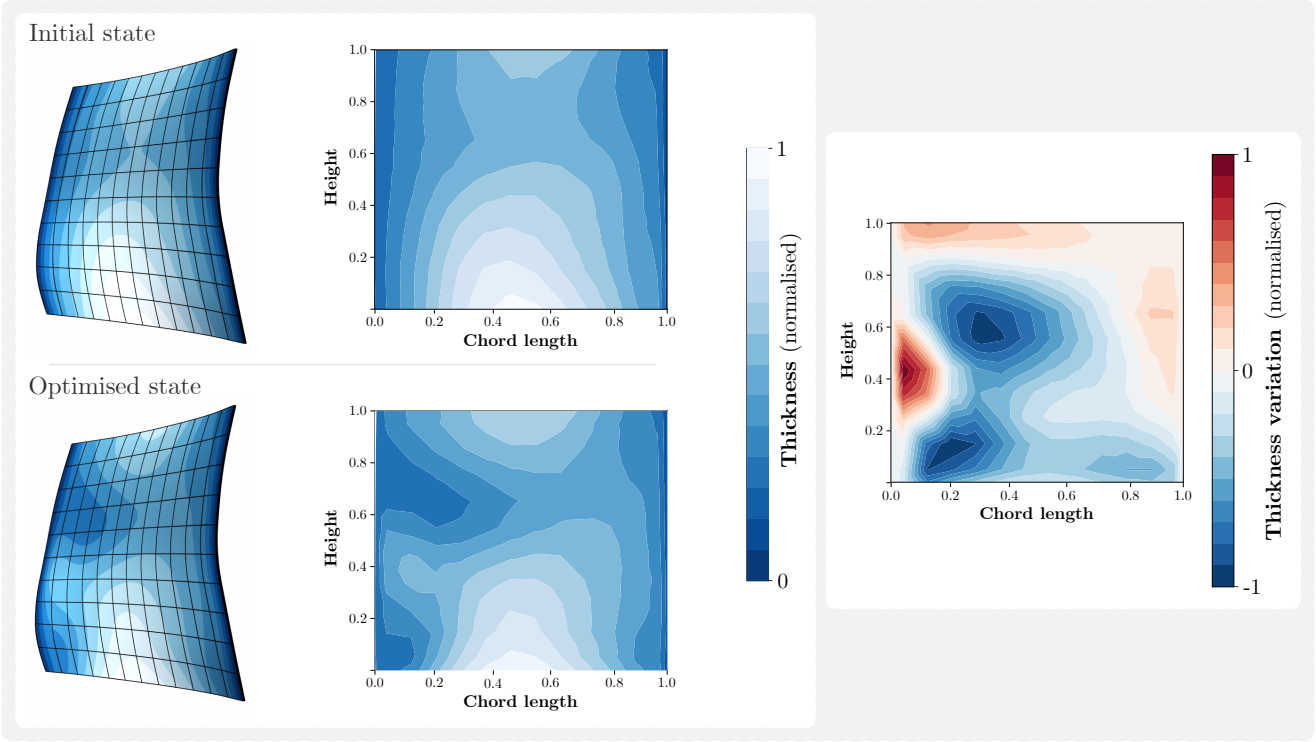

Fig. 15: Left: thickness contour plot of the HP compressor blade, plotted onto the geometry and in a flattened space. Right: thickness variation between the two states, represented in a flattened space. The thickness values correspond to the one defined for the shape parametrisation.

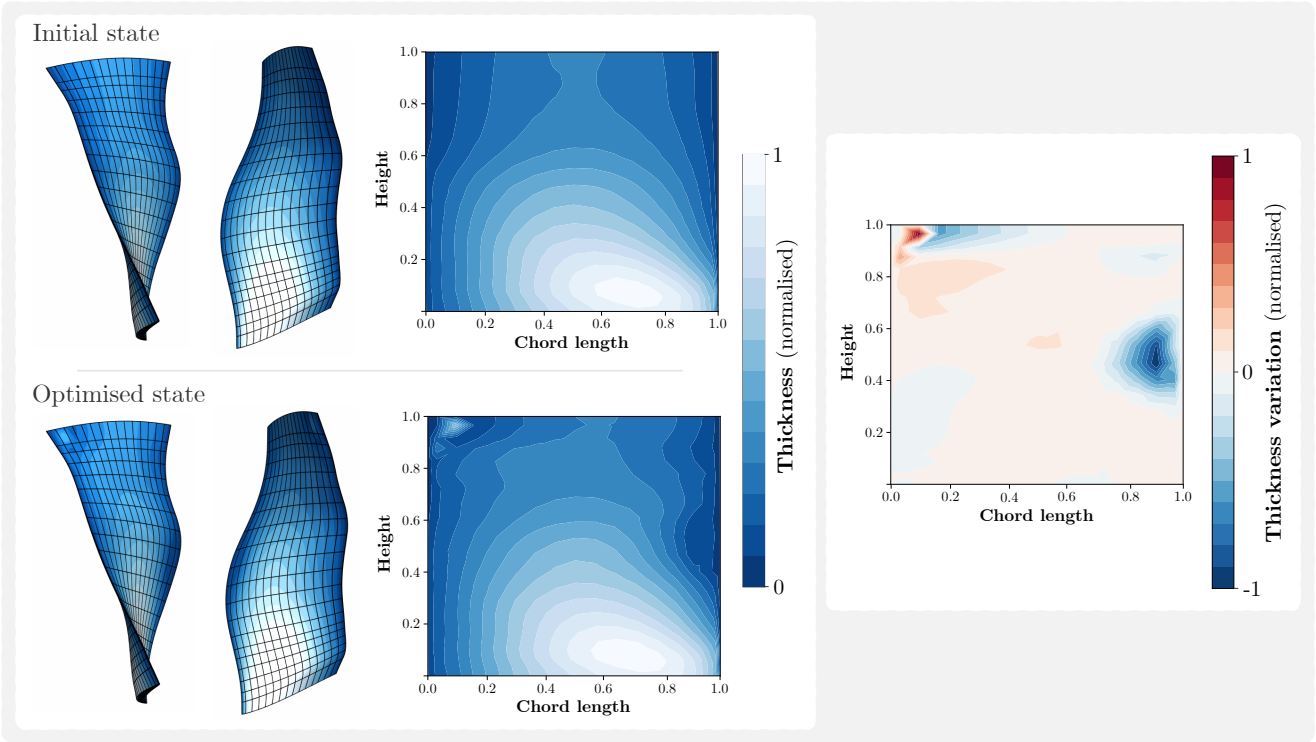

Fig. 16: Left: thickness contour plot of the fan blade, plotted onto the geometry and in a flattened space. Right: thickness variation between the two states, represented in a flattened space. The thickness values correspond to the one defined for the shape parametrisation.

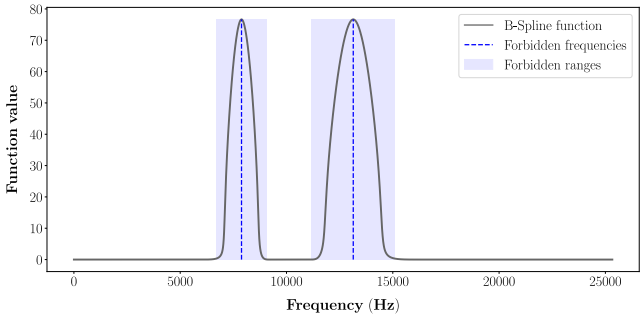

Fig. 17: Example of B-Spline penalty function. High function values are set near the forbidden frequencies, and low values are set elsewhere.

Our proposal is to use a combination of B-spline curves as a penalty function (see figure 17). High penalty values are set in the vicinity of forbidden frequencies of interest, and zero values are set elsewhere. To achieve this, the B-spline curve is defined as a sum of "bumped" function that are B-spline curves themselves. The interest of using a sum of B-Spline functions as a penalty function is multiple. First, it is easy to define a function that presents the desired aspect for our application. Then, B-Spline continuity and differentiability allows to compute analytically the gradient values of the resulting objective function. Hence, using a B-Spline definition is interesting in the analytic framework we set up.

To demonstrate the effectiveness of this objective function, we consider two forbidden frequency ranges for each blade: the 30N and 50N harmonics are chosen for the HP compressor blade, and the 1N and 2N harmonics are chosen for the fan blade (see figure 10). The rest of the optimisation set-up is the same as in section 5.3 for both blades.

We first look into the results obtained for the HP compressor blade. The evolution of the values of the first ten natural frequencies during the optimisation is presented in figure 18a. In the initial state, two natural frequencies are lying in two different forbidden ranges (iteration 0). An optimum is reached after 11 iterations. No more natural frequency lies in the forbidden ranges, and the volume constraint is respected. The final volume value lies on the upper limit we set for the constraint, *i.e.* 10% greater than the initial one.

Figure 18b shows the evolution of the objective function and constraint values over the iterations. Thickness contour plots are presented in figure 20. It can be observed that the objective function reaches a minimum after 4 iterations, and that subsequent iterations are necessary to satisfy the volume constraint.

We now turn to the results for the fan blade. The optimisation histories for this case are presented in figure 19. In this case four natural frequencies lie in the forbidden frequency ranges at the beginning. An optimum is reached after

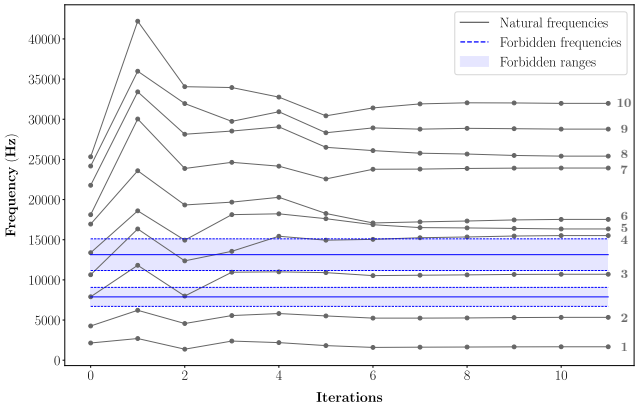

(a) Evolution of the first ten natural frequencies across the optimisation.

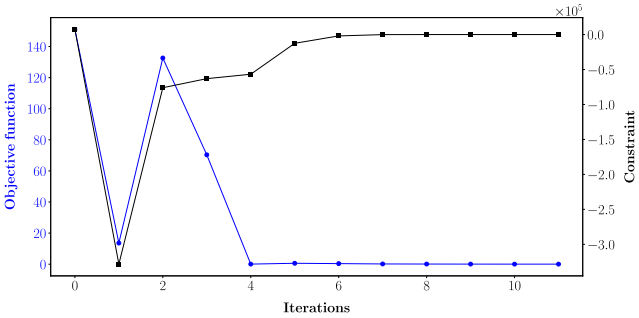

(b) Evolution of the objective function and constraint values over the optimisation.

Fig. 18: Optimisation histories for the second vibration case on the HP compressor blade.

17 iterations, the constraint being respected throughout the whole optimisation procedure. The thickness contour plots are presented in figure 21. It can be observed that the magnitude of the thickness modifications is larger in this case than in the target frequencies case – this aspect can be observed by comparing the *Thickness variation* plots of both cases. The volume is however overall similar to the initial one, the increase being of 2%.

6 Conclusions

This article presents first steps towards a methodology for the parametric shape optimisation of aircraft engines axial compressor blades using isogeometric analysis (IGA). Its contribution is two-fold.

First, a procedure to generate analysis- and optimisation-suitable volumetric B-spline models starting from stacked blade profiles is proposed. Its effectiveness is demonstrated on a small and thick high-pressure compressor blade and on a more slender and twisted low-pressure compressor fan blade. It is our belief that the proposed methodology can

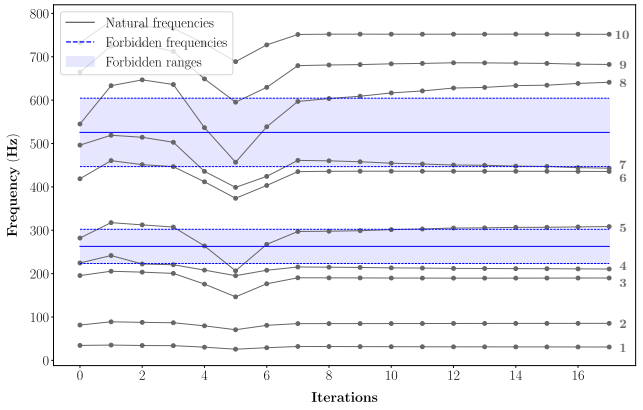

(a) Evolution of the first ten natural frequencies across the optimisation.

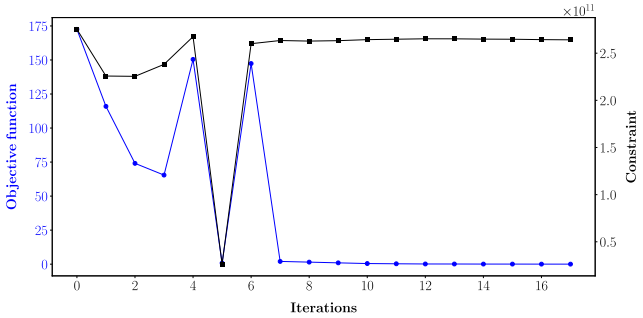

(b) Evolution of the objective function and constraint values over the optimisation.

Fig. 19: Optimisation histories for the second vibration case on the fan blade.

generalise to other blade shapes, such as propeller blades or turbine blades.

Secondly, we investigate different optimisation problem formulations to solve two different sizing cases. The first case is based on a static analysis featuring a centrifugal force and an actual surface pressure field coming from aerodynamic simulations. The objective is to reduce the overall blade displacements in that case. To this end, a differentiable parametric stacking law modification procedure is setup and a compliance minimisation under volume and bounds constraints formulation is used. It is shown that a 40% compliance drop can be achieved in this case, effectively reducing the overall displacements.

The second case uses a dynamic analysis and is based on Campbell diagrams. The objective is to concurrently satisfy several frequency margins specifications. A differentiable parametric thickness modification procedure is setup in this case and two objective function formulations are considered. The first formulation is a classical target attainment formulation. It is shown that target frequencies can indeed be reached if appropriately set. Satisfying results are obtained with this formulation but has limitations. Indeed, it is not practical when a high number of natural frequencies have to be constrained, or when it is desirable to avoid multiple frequency ranges simultaneously. To circumvent these limitations, a forbidden frequencies ranges formulation with a B-spline based objective function definition is proposed. It is shown that this formulation effectively lifts the aforementionned limitations.

Several directions for future research can be envisionned. First, the representativeness of our calculations could be improved. Although centrifugal forces are taken into account in the static calculations we perform, these are not accounted for in the dynamic analysis. However, it is known that blades tend to stiffen under centrifugal forces, which renders its natural frequencies dependent on the rotation speed of the engine.

Also, we limited ourselves to embedded blades in this work, which prevented us from studying structural constraints, which have a major impact on blades life expectancy and therefore on their sizing. A more involved model integrating both the blade and its platform would be required to accurately simulate the force paths passing through the blade root. This should be the object of our future research.

Finally, another aspect that we did not investigate in this work is the possibility of using different optimisation algorithms. Satisfying results were obtained with the one that we considered, but reductions of the overall optimisation time could probably be achieved with a better choice of algorithm and/or a better tuning of the optimisation algorithm parameters. Gradient-based methods are favoured in our framework, since analytical sensitivities can be computed. Investigating the benefit of multi-start methods is another perspective of this work.

Compliance with ethical standards

Conflict of interest

The authors declare that they have no conflict of interest.

Replication of results

Additional data and computer codes cannot be shared due to commercial or technical secrets considerations.

References

A. Arapakopoulos, R. Polichshuk, Z. Segizbayev, S. Ospanov, A. I. Ginnis, and K. V. Kostas. Parametric models for marine propellers. 2019.

C. H. Bischof, H. M. Bücker, P. Hovland, U. Naumann, and J. Utke, editors. *Advances in automatic differentiation*. 2008.

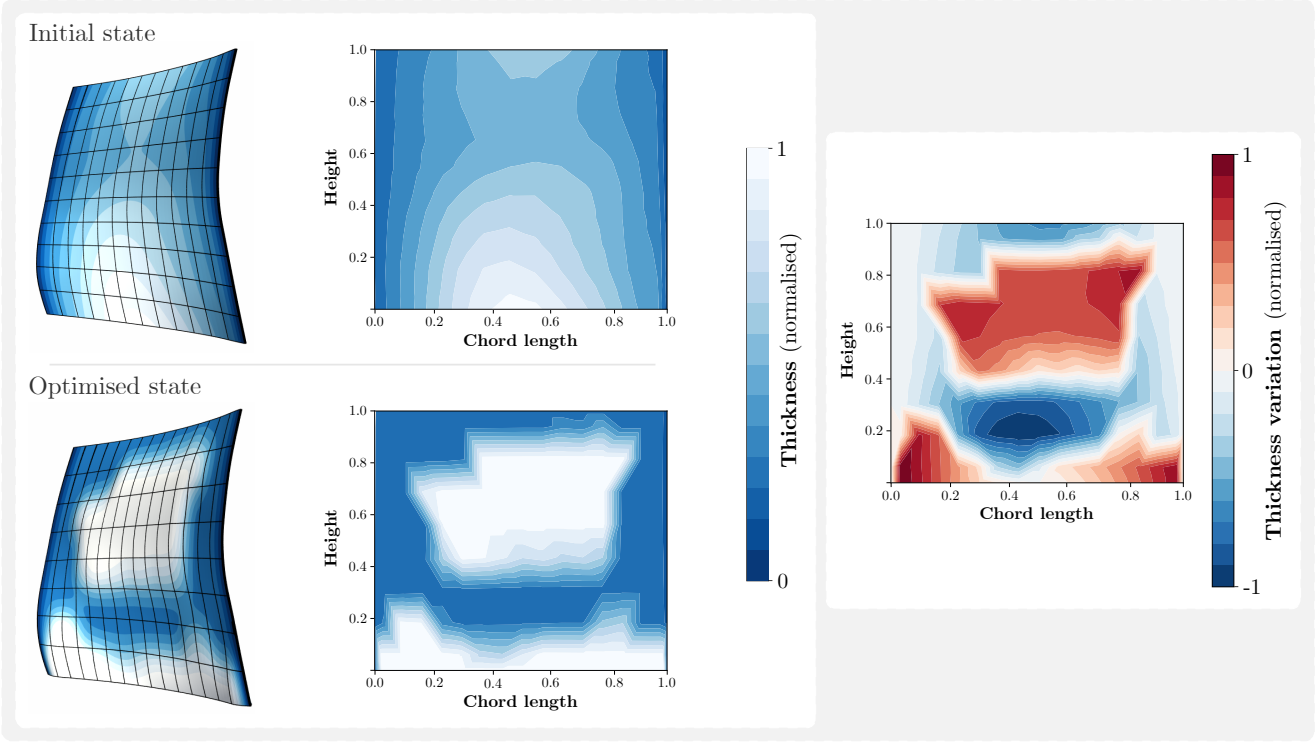

Fig. 20: Left: thickness contour plot of the fan blade, plotted onto the geometry and in a flattened space. Right: thickness variation between the two states, represented in a flattened space. The thickness values correspond to the one defined for the shape parametrisation.

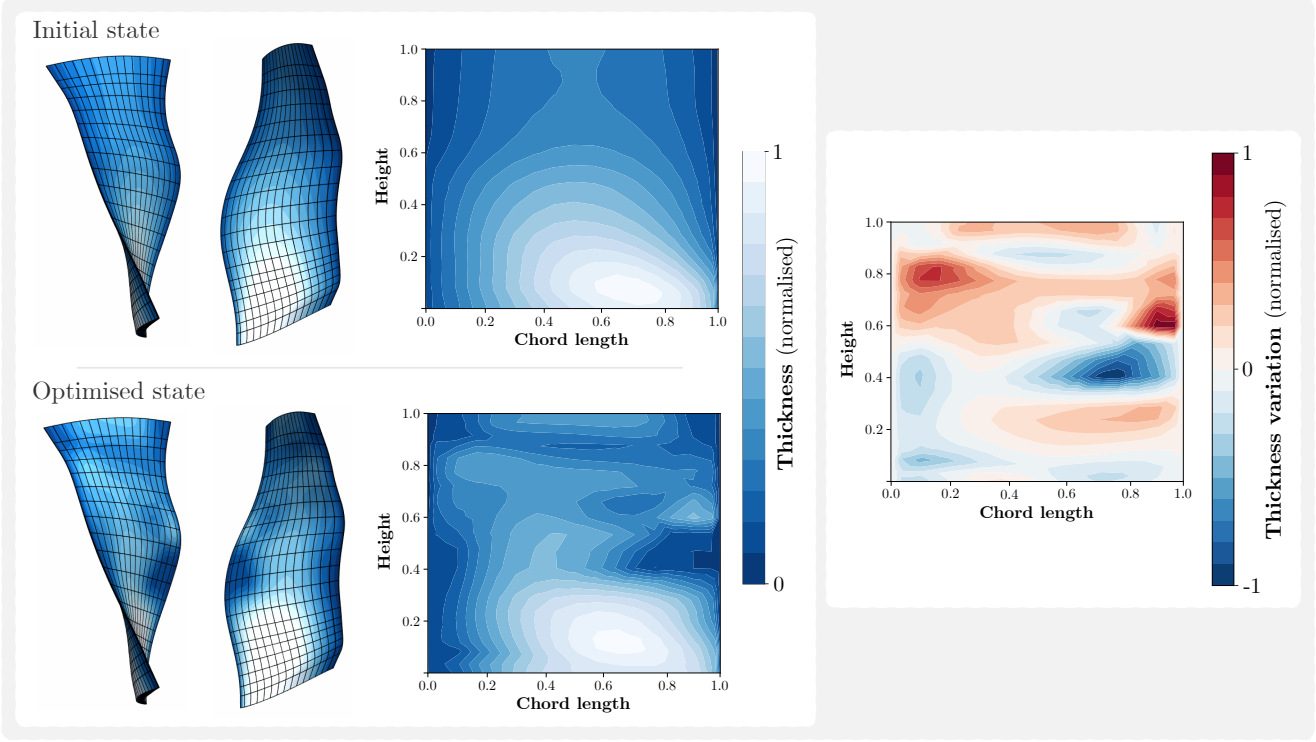

Fig. 21: Left: thickness contour plot of the fan blade, plotted onto the geometry and in a flattened space. Right: thickness variation between the two states, represented in a flattened space. The thickness values correspond to the one defined for the shape parametrisation.

L. Blanchard, R. Duvigneau, A.-V. Vuong, and B. Simeon. Shape Gradient Computation in Isogeometric Analysis for Linear Elasticity. Technical report, INRIA, 2012.

K.-U. Bletzinger. A consistent frame for sensitivity filtering and the vertex assigned morphing of optimal shape. 49: 873–895, 2014.

V. Braibant and C. Fleury. Shape optimal design using B-Splines. *Computer methods in applied mechanics and engineering*, 44:247–267, 1984.

M. Bücker, G. Corliss, P. Hovland, U. Naumann, B. Norris, T. J. Barth, M. Griebel, D. E. Keyes, R. M. Nieminen, D. Roose, and T. Schlick, editors. *Automatic Differentiation: Applications, Theory, and Implementations*, volume 50. Springer Science & Business Media, 2006.

W. Campbell. Protection of Turbine Disk Wheels from Axial Vibration. In *Protection of steam turbine disk wheels from axial vibration*. General electric Company, 1924.

S. Cho and S. H. Ha. Isogeometric shape design optimization: Exact geometry and enhanced sensitivity. *Structural and Multidisciplinary Optimization*, 38(1):53–70, 2009.

S. A. Coons. Surfaces for Computer-Aided Design of space forms. Technical report, Massachusetts Institute of Technology, Cambridge, Massachusetts, 1967.

J. A. Cottrell, T. J. R. Hughes, and A. Reali. Studies of refinement and continuity in isogeometric structural analysis. 2007.

J. A. Cottrell, T. J. R. Hughes, and Y. Bazilevs. *Isogeometric Analysis*. John Wiley & Sons, Ltd, Chichester, UK, 2009.

M. G. Cox. The numerical evaluation of B-Splines. *IMA Journal of Applied Mathematics (Institute of Mathematics and Its Applications)*, 10(2):134–149, oct 1972.

C. De Boor. On Calculating with BSplines. *Journal of Approximation Theory*, 1(6):50–62, 1972.

C. S. Ding, X. Y. Cui, and G. Y. Li. Accurate analysis and thickness optimization of tailor rolled blanks based on isogeometric analysis. *Structural and Multidisciplinary Optimization*, 54(4):871–887, 2016.

G. Farin and D. Hansford. Discrete Coons patches. *Computer Aided Geometric Design*, 16:691–700, 1999.

M. Firl, R. Wüchner, K.-U. Bletzinger, M. Firl, R. Wüchner, and K.-u. Bletzinger. Regularization of shape optimization problems using FE-based parametrization. 47:507–521, 2013.

D. Fußeder, B. Simeon, and A.-V. Vuong. Fundamental aspects of shape optimization in the context of isogeometric analysis. *Computer Methods in Applied Mechanics and Engineering*, 286:313–331, 2015.

D. Großmann and B. Jüttler. Volumetric Geometry Reconstruction of Turbine Blades for Aircraft Engines. In J.-D. Boissonnat, P. Chenin, A. Cohen, C. Gout, T. Lyche, M.-L. Mazure, and L. Schumaker, editors, *International Conference on Curves and Surfaces*, pages 280–295, Berlin, Heidelberg, 2010. Springer.

Y. D. Ha. Generalized isogeometric shape sensitivity analysis in curvilinear coordinate system and shape optimization of shell structures. *Structural and Multidisciplinary Optimization*, 52(6):1069–1088, 2015.

V. Hernández-Mederos and J. Estrada-Sarlabous. Sampling points on regular parametric curves with control of their distribution. *Computer Aided Geometric Design*, 20(6): 363–382, 2003.

A. J. Herrema, N. M. Wiese, C. N. Darling, B. Ganapathysubramanian, A. Krishnamurthy, and M. C. Hsu. A framework for parametric design optimization using isogeometric analysis. *Computer Methods in Applied Mechanics and Engineering*, 316:944–965, 2017.

T. Hirschler, R. Bouclier, A. Duval, T. Elguedj, and J. Morlier. Isogeometric sizing and shape optimization of thin structures with a solid-shell approach. *Structural and Multidisciplinary Optimization*, 59(3):767–785, 2018.

T. Hirschler, R. Bouclier, A. Duval, T. Elguedj, and J. Morlier. A New Lighting on Analytical Discrete Sensitivities in the Context of IsoGeometric Shape Optimization. *Archives of Computational Methods in Engineering*, pages 1–38, sep 2020.

M. C. Hsu, C. Wang, A. J. Herrema, D. Schillinger, A. Ghoshal, and Y. Bazilevs. An interactive geometry modeling and parametric design platform for isogeometric analysis. *Computers and Mathematics with Applications*, 70(7):1481–1500, 2015.

T. J. R. Hughes, J. A. Cottrell, and Y. Bazilevs. Isogeometric analysis: CAD, finite elements, NURBS, exact geometry and mesh refinement. *Computer Methods in Applied Mechanics and Engineering*, 194(39-41):4135–4195, 2005.

M. H. Imam. Three-dimensional shape optimization. *International Journal for Numerical Methods in Engineering*, 18(5):661–673, may 1982.

P. Kang and S. K. Youn. Isogeometric shape optimization of trimmed shell structures. *Structural and Multidisciplinary Optimization*, 53(4):825–845, 2016.

J. Kiendl, R. Schmidt, R. Wüchner, and K. U. Bletzinger. Isogeometric shape optimization of shells using semi-analytical sensitivity analysis and sensitivity weighting. *Computer Methods in Applied Mechanics and Engineering*, 274:148–167, 2014.

D. Kraft. Algorithm 733: TOMP-Fortran Modules for Optimal Control Calculations. *ACM Transactions on Mathematical Software (TOMS)*, 20(3):262—-281, 1994.

H. Liu, D. Yang, X. Wang, Y. Wang, C. Liu, and Z. P. Wang. Smooth size design for the natural frequencies of curved Timoshenko beams using isogeometric analysis. *Structural and Multidisciplinary Optimization*, 59(4): 1143–1162, 2019.

O. Mykhaskiv, M. Banovic, S. Auriemma, P. Mohanamuraly, A. Walther, H. Legrand, and J.-D. Müller. NURBS-based and Parametric-based Shape Optimisation with

Differentiated CAD Kernel. Technical report, 2018.

A. P. Nagy, M. M. Abdalla, and Z. Gürdal. Isogeometric sizing and shape optimisation of beam structures. *Computer Methods in Applied Mechanics and Engineering*, 199(17-20):1216–1230, 2010.

A. P. Nagy, M. M. Abdalla, and Z. Gürdal. Isogeometric design of elastic arches for maximum fundamental frequency. *Structural and Multidisciplinary Optimization*, 43(1):135–149, 2011.

J. Nocedal and S. Wright. *Numerical optimization*. Springer Science & Business Media, 2006.

F. Pérez-Arribas and R. Pérez-Fernández. A B-spline design model for propeller blades. 2018.

L. Piegl and W. Tiller. *The NURBS book*. Springer, Berlin, Heidelberg, 1995.

X. Qian. Full analytical sensitivities in NURBS based isogeometric shape optimization. *Computer Methods in Applied Mechanics and Engineering*, 199(29-32):2059–2071, jun 2010.

P. Stein, M. C. Hsu, Y. Bazilevs, and K. E. Beucke. Operator- and template-based modeling of solid geometry for Isogeometric Analysis with application to Vertical Axis Wind Turbine simulation. *Computer Methods in Applied Mechanics and Engineering*, 213-216:71–83, 2012.

P. Virtanen, R. Gommers, T. E. Oliphant, M. Haberland, T. Reddy, D. Cournapeau, E. Burovski, P. Peterson, W. Weckesser, J. Bright, S. J. van der Walt, M. Brett, J. Wilson, K. J. Millman, N. Mayorov, A. R. J. Nelson, E. Jones, R. Kern, E. Larson, C. Carey, l. Polat, Y. Feng, E. W. Moore, J. VanderPlas, D. Laxalde, J. Perktold, R. Cimrman, I. Henriksen, E. A. Quintero, C. R. Harris, A. M. Archibald, A. H. Ribeiro, F. Pedregosa, P. van Mulbregt, and S. . . Contributors. SciPy 1.0–Fundamental Algorithms for Scientific Computing in Python. *Nature Methods*, jul 2020.

W. A. Wall, M. A. Frenzel, and C. Cyron. Isogeometric structural shape optimization. *Computer Methods in Applied Mechanics and Engineering*, 197(33-40):2976–2988, 2008.

G. Xu, B. Mourrain, R. Duvigneau, and A. Galligo. Parameterization of computational domain in isogeometric analysis: Methods and comparison. *Computer Methods in Applied Mechanics and Engineering*, 200(23-24):2021–2031, 2011.